Rijksuniversiteit Groningen

Bachelor Thesis

Enviromental Star Formation Suppression in Galaxy Clusters

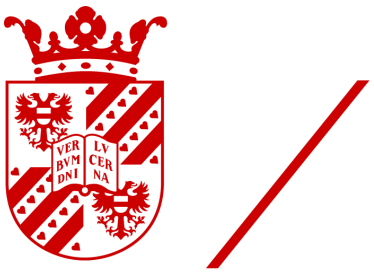

university of groningen

Author:
Anatolii I. Zadvornyi

Supervisors:
dr. Kyle A. Oman
prof. dr. Marc A.W. Verheijen

July 5, 2019

Contents

Abstract

Quenching timescale τ_q as a function of stellar mass was calculated using the EAGLE simulation to see if we could find similar trends as in Fillingham *et al.* (2015). For satellites with stellar masses of $\log_{10}(M_\star/M_\odot) = [9, 11]$: we have found a peak in τ_q–$M_\star$ relation for intermediate mass satellites, at $\log_{10}(M_\star/M_\odot) \approx 10$; negative slope is observed for higher mass satellites $\log_{10}(M_\star/M_\odot) > 10$; positive slope for lower mass satellites, $\log_{10}(M_\star/M_\odot) < 10$. We have also shown that orbital properties (M_{host}, v_{peri} and r_{peri}) can dramatically affect τ_q while preserving the general trend. Similarly, internal properties $R_{half,\star}$ and $M_{gas}/M_\star$ suggest that higher and lower stellar mas satellites are dominated by different quenching mechanisms: RPS for lower masses, strangulation for higher masses. It appears that intermediate masses can effectively resist RPS, while having enough gas in their reservoirs to not be strangled by ICM for the next ≈ 6 Gyr after infall.

1 Introduction

1.1 Groups and Clusters

Satellite galaxies are those which orbit much more massive galaxies or clusters of galaxies. Collections of galaxies are often classified as either 'groups' that contain tens of galaxies, such as our Local Group, or clusters, which contain hundreds of galaxies, for example, the Virgo Cluster. These large clusters are thought to be responsible for the decrease of star formation rate (SFR) in satellites (Dressler 1980; Baldry *et al.* 2006; Wetzel *et al.* 2013). There are a few indicators of such behaviour: (i) spiral galaxies can only be formed in the field environment, since the timescale of disc formation is several Gyr and the cluster environment can halt or even remove the gas from the disc on the same timescale. It was observed (Butcher and Oemler 1984) in nearby clusters that spirals have, on average, redder bulge than the field ones which indicates that the infall of gas was halted. The spirals are also bluer than ellipticals due to young OB stars that are formed in the gas rich regions of spirals. Since the lifetime of OB stars are a few tens of Myr, the large count of them indicates a region with considerable amount of gas; (ii) morphology is another strong indicator of gas abundance in a galaxy. Generally, elliptical galaxies are gas poor and hence they cannot support creation of stars. Since solar mass stars live much longer and are red in colour, ellipticals are also red. It was shown (Postman and Geller 1984; Gunn and Gott 1972) that high galaxy density regions are dominated by ellipticals.

Cluster environment star formation suppression is a known phenomenon but the details of which physical mechanisms drive quenching as a function of satellite stellar mass is not yet fully understood. Fillingham *et al.* (2015) showed (see Fig. 1) that the quenching timescale (which is explained in the next section) is dependant on the stellar mass of the satellite and independent of the host mass. Points in Fig. 1 correspond to measurements of satellites around hosts of different masses, which will make interpretation slightly more difficult. Satellites, starting from $\log_{10}(M_\star/\mathrm{M}_\odot) \approx 6$ have an increasing quenching timescale up until $\mathrm{M}_{\mathrm{crit}}$ at around $\log_{10}(M_\star/\mathrm{M}_\odot) \approx 9$, after which the quenching timescale decreases with increasing solar mass of the satellite. In this thesis we will attempt explain this rather peculiar peak: intermediate mass satellites seem to be very effective at keeping their gas while travelling through intra-cluster medium (ICM). The EAGLE simulation (Schaye *et al.* 2015; Crain *et al.* 2015) was used to examine galactic evolution.

1.2 Quenching

There are, roughly speaking, three phases though which gas passes in order to form a new star. They differ by temperature, density, ionizastion state and location. Starting from outer regions – galactic corona. It contains hot $T \approx 10^6$ K, tenuous $n \approx 10^{-3}$ cm^{-3} ionized hydrogen, fueled by galactic fountains and warm intergalactic streams (Fraternali and Binney 2008; Oort 1970). As coronal gas cools down and rains back into galactic disc entering warm neutral state, with temperatures of $T \approx 10^4$ K and densities n ≈ 0.2 cm^{-3}. From here, it can be blown back into corona by strong solar winds and supernovae feedback or it can cool down further to form molecular clouds. The clouds have typical temperatures of $T \approx 10$ K and densities $n > 10^3$ cm^{-3}. Inner unstable regions of molecular clouds can collapse to form stars. A fraction of H_2 will be photodissociated and fed back into the warm neutral medium. OB stars can blow out surrounding gas even further into the corona, known as "galactic wind", and then undergo supernova, to blast the surrounding gas from the plane of the disc back to the corona.

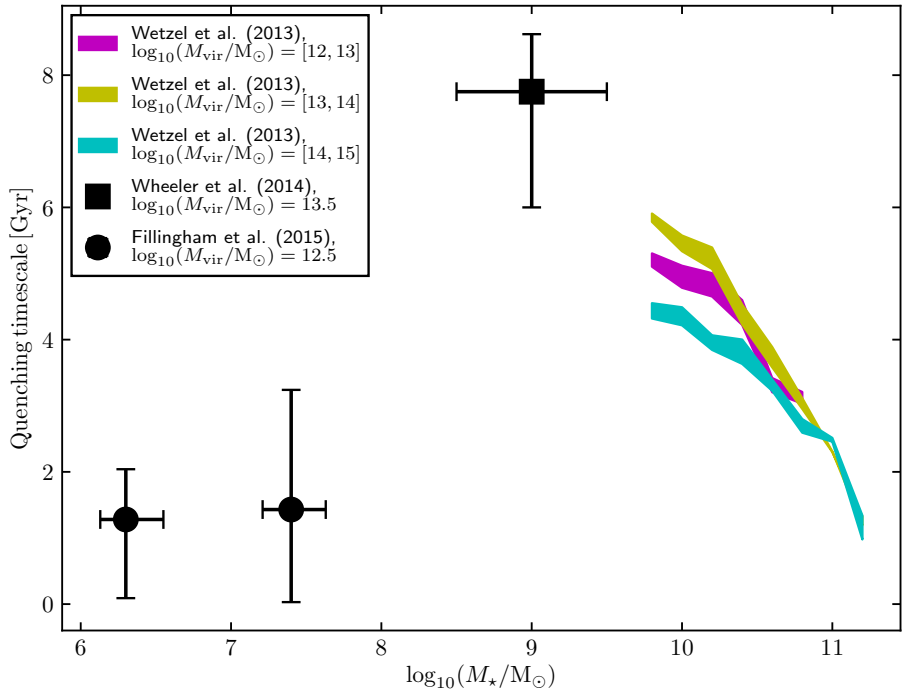

Figure 1: Quenching timescale as a function of satellite stellar mass, reproduced from Fillingham *et al.* (2015). Quenching timescale is relatively low for "low" mass satellites $\log_{10}(M_\star/{\rm M}_\odot) \approx [6, 8]$ and for "high" mass satellites $\log_{10}(M_\star/{\rm M}_\odot) \approx [10, 11]$. However, the quenching timescale for "intermediate" mass satellites, $\log_{10}(M_\star/{\rm M}_\odot) \approx [8, 10]$ is considerably higher, compared to low and high mass satellites. There appears to be a trend for the quenching timescale to grow from low mass satellite up to a critical mass $\rm M_{crit}$ and then decline afterwards. This suggests that the quenching of satellites of different masses are affected by different mechanisms.

There are several ways to halt production of stars, for instance (i) deplete H_2 reservoir and prevent HI $\longrightarrow$ H_2 transition, (ii) deplete HI $\longrightarrow$ H_2 and H_2 and prevent H^+ $\longrightarrow$ HI or (iii) remove H^+ and HI and deplete H_2. These scenarios are governed by (a combination of) different mechanisms that act on dissimilar timescales. Postman and Geller (1984) suggest that the main quenching mechanism in play depends on the mass of the satellite. That is, lighter satellites are affected by ram-pressure stripping or some other mechanism (quenching mechanisms are explained in detail later in this section), which removes the HI reservoirs. More massive satellites, on the other hand, may be affected by strangulation, which prevents coronal accretion of intergalactic hot gas.

Galaxies can be divided into two categories based on their location in a colour-magnitude diagram. Thriving ones with many OB stars produced are classified as a part of the "blue cloud" (Blanton *et al.* 2003; Ghosh *et al.* 2019). Likewise, those which stopped star formation and have their OBs long gone fall on the "red sequence" (Baum 1959). The much more weakly populated transition region between the blue cloud and the red sequence is called the "green valley". If, for one reason or another, the used up gas is not replenished or existing one is removed, new stars cannot be formed, and we say that a galaxy is "quenched". To quantify this, we refer to specific star formation rates, SSFR = SFR/$\rm M_\star$ that have value of $\log_{10}({\rm SSFR/yr}^{-1}) \leq -11.0$. This is the upper boundary of SSFR in the "red sequence". In simulations, like the one we used, low SSFRs can be as low as zero. They can not be shown on the $\log_{10}$ scale. All the satellites with non-zero SSFR at z = 0 can be seen in Figure 2. The red sequence in the simulation we used

contains 58% of galaxies with stellar masses of $M_\star > 10^9$.

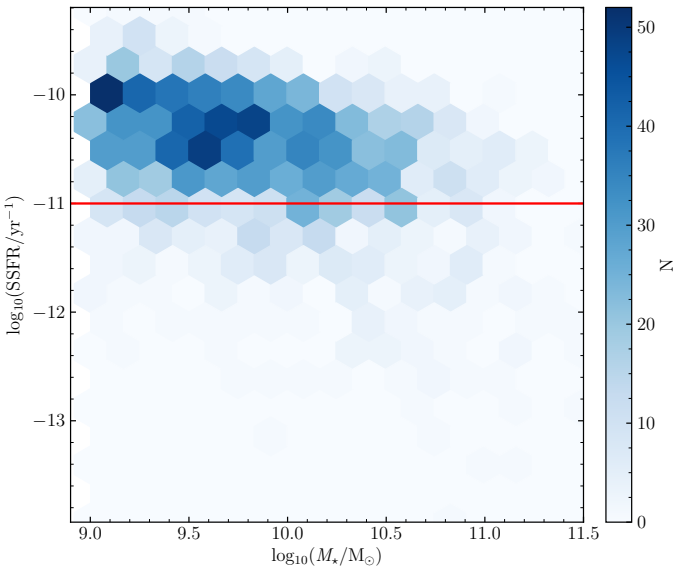

Figure 2: SSFR of satellites as a function of stellar mass in one of EAGLE simulations, specifically of REFL0100N1504 run at z = 0. A galaxy is considered to be quenched if it lies in the region $\log_{10}(\mathrm{SSFRcut/yr^{-1}}) \leq -11.0$. The blue cloud can be clearly seen, but the red sequence is seemingly absent, since 0 can not be represented on a log scale. 58% of satellites in this run have SSFR = 0 at $z = 0$.

1.2.1 Ram-pressure stripping

Description of the following quenching mechanisms (and simulations in section 1.3) is based on the overview in Oman (2013). Reduction of SSFR in a galaxy can be driven by both internal and external processes. One of the external mechanisms is ram pressure stripping (RPS):

$$P_{\mathrm{ram}} \approx \rho_{\mathrm{ICM}}(r_{\mathrm{c}})|v^2| \tag{1}$$

where $\rho_{\mathrm{ICM}}(r_{\mathrm{c}})$ is the density of the intra-cluster medium at a radius r_c from the centre of the cluster and $|v|$ is the relative speed of the satellite galaxy with respect to the ICM. It affects the disc of a galaxy and depends on the angle of attack: RPS is more effective if the disc is oriented face-on relative to the movement. From the equation above it can be seen that RPS is more effective in higher density environments and at higher speeds, that is during pericentric approach of a satellite.

Gunn and Gott (1972) suggested a simple model for the restoring gravitational force per unit area:

$$\mathfrak{F} = 2\pi G \Sigma_{\mathrm{g}} \Sigma_{\mathrm{s}} \tag{2}$$

where G is gravitational constant and Σ_{g} and Σ_{s} are the surface density of the gas and stars of the galaxy respectively. The stripping occurs when the ram-pressure overcomes the gravitational pull of the galaxy onto the gas in the disc:

$$\rho_{\mathrm{ICM}}(r_{\mathrm{c}})|v^2| > 2\pi G \Sigma_{\mathrm{g}} \Sigma_{\mathrm{s}} \tag{3}$$

1.2.2 Tidal stripping

Another external quenching mechanism is tidal stripping. It is a force exerted by a cluster on a satellite which is stronger on the near side of the satellite compared to the far side. Dark matter halo falls victim to tidal stripping first, since it is weakly bound, followed by coronal gas. And in cases of particularly strong fields, gas and stars can be siphoned out from the disc of a galaxy. For idealised spherically symmetric host and satellite, condition for tidal stripping can be estimated. To first order, the acceleration felt by a particle in the tidal field, along the axis joining the centre of the host and satellite, is given by:

$$a_{\text{tidal,axial}} = \frac{2rGM_{\text{host}}(< R)}{R^3}, \tag{4}$$

where r is the distance from the centre of the satellite, R is the radial separation between the centre of the cluster and the centre of the satellite and M_{host} is the mass of the cluster. Hence, in order for tidal stripping to occur, it must exceed the gravitational pull of the satellite on the particle:

$$\frac{GM_{\text{sat}}(< r)}{r^2} < \frac{2rGM_{\text{host}}(< R)}{R^3}, \tag{5}$$

which can be expressed in terms of mean densities:

$$\bar{\rho}_{\text{sat}}(< r) < \bar{\rho}_{\text{host}}(< R). \tag{6}$$

The last inequality illustrates that tidal stripping will carry on until the density of the satellite becomes of the order of that of the environment it is falling through. Even if tidal forces cannot directly remove the material from a satellite galaxy, they can enhance other mechanisms. For example, tidal heating can inject energy to the gas making it easier for the ram-pressure to remove more gas.

1.2.3 Strangulation

Oort (1970) and Larson *et al.* (1980) argued that since the consumption rate of a typical spiral is much shorter the Hubble time, the gas reservoirs must be replenished for the continuous formation of stars. Strangulation is a mechanism that halts gas supply in one way or another until all the fuel for star formation is depleted (different scenarios are discussed in the beginning of this section). Strangulation can be caused by interaction of the satellite with ICM or another, similar sized galaxy in much smaller groups.

1.2.4 Internal mechanisms

There are few ways a galaxy can halt or reduce its own SFR. Supernovae can put an upper limit on SFR in gas rich environments where OB stars can be born. Since OB stars are short-lived and have the same order of magnitude timescale as a protostar to enter the main sequence, supernovae events will disrupt nearby molecular clouds that would otherwise form a star, thus self-regulating SFR.

AGN feedback is another self-regulating mechanism, that injects energy to the nearby gas clouds, preventing them from collapsing, or blows the clouds away altogether. After the material has been displaced from the vicinity of the BH, it can no longer fuel the AGN and hence the process stops until the next cycle (Morganti 2017).

1.3 Simulations

To probe the structure and distribution of galaxies computer simulations can be used. They are an approximate solution to N-body and Smoothed Particle Hydrodynamics equations:

$$\vec{F_i} = \sum_{i \neq n}^{N} \frac{G m_n m_i}{r_{ni}^2} \hat{r}_{ni} \tag{7}$$

and

$$m_i \frac{\mathrm{d}\mathbf{v}_i}{\mathrm{d}t} = -\sum_{j=1}^{N} x_i x_j \left[\frac{P_i}{y_i^2} f_{ij} \nabla_i W_{ij}(h_i) + \frac{P_j}{y_j^2} f_{ji} \nabla_i W_{ji}(h_j) \right] \tag{8}$$

which are explained in detail by Schaye *et al.* (2015) and Springel (2005).

To simulate the behaviour of fluid, the particle distribution must first be discretized and then all the forces that act on those particles must be computed in order to advance to the next time step. In the end there will be a final snapshot with galaxies and clusters of galaxies distributed over the cosmic web. The collection of individual galaxies are grouped (at every snapshot), based on their vicinity to each other. Friends-of-Friends (FoF) group-finding algorithm is used: a particle belongs to a FoF group (which has a unique id) if it is within some linking length l of any other particle in the group; if a group has fewer than n members, it is rejected (Quinn *et al.* 2000). Then, within each FoF group a subfind algorithm is used to identify gravitationally bound clumps of matter – galaxies. In the case of groups and clusters, all galaxies within the group/cluster usually belong to the same FoF group. The heaviest galaxy in FoF group is assigned as a "host" galaxy. Every host galaxy has a `SubGroupNumber = 0` and all its satellites have `SubGroupNumber > 0`. Using this classification, host galaxies and their satellites can be selected in order to examine their history and, perhaps, find events and key parameters that could explain their final properties – quenching timescale τ_{q} as a function of stellar mass $M_\star$ in our case.

2 Methods

2.1 The EAGLE simulations

The Virgo consortium's **E**volution and **A**ssembly of **G**a**L**axies and their **E**nvironments is a hydrodynamical simulation developed to study the formation and evolution of galaxies on cosmic scales which uses periodic boundary conditions. The following cosmological parameters are used (Planck Collaboration *et al.* 2014): $\Omega_M = 0.307$, $\Omega_\Lambda = 0.693$, $\Omega_b = 0.04825$, $h = 0.6777$, $\sigma_8 = 0.8288$, $n_s = 0.9611$, $Y = 0.248$. The simulation, among all the kinematic and cosmological calculations, includes the following physical processes: star formation, stellar evolution, metal enrichment, feedback from stars, seeding and growth by accretion and merging of supermassive black holes and feedback from accreting black holes (The EAGLE team 2017).

Simulations differ by resolution, particle number and box sizes. For example, one of the simulations we used was RefL0100N1504, which refers to simulation box of size L = 100 comoving Mpc (cMpc) and starts with 2×1504^3 (dark matter and gas) particles. There are 29 snapshots (from $z = 20$ to $z = 0$). To track evolution of a galaxy, a merger tree is built. The heaviest branch, called trunk, links the final galaxy to its main progenitor at earlier times. Properties of the galaxy and all the mergers it experienced can be reconstructed. An example of a merger tree can be seen in Fig 3.

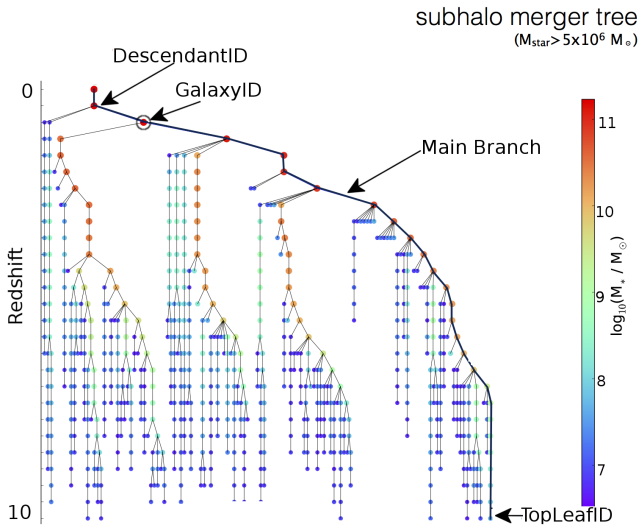

Figure 3: A typical merger tree in EAGLE simulation, reproduced from McAlpine *et al.* (2016). The trunk (main branch) is the rightmost branch of the tree. All the mergers and sub-mergers can be seen to the left of the trunk.

We selected a sample of host galaxies, which have dark matter halo mass of $M_{\rm DM}/{\rm M}_\odot > 10^{13}$. In REFL0100N1504 simulation there were 168 such galaxies. Then, we selected satellite galaxies with mass range $10^9 < M_\star/{\rm M}_\odot < 10^{12}$ that were in the proximity of respective hosts at $z = 0$. Proximity is defined as a box with the host galaxy in the centre and with a side of $l = 2 \times 3.3{\rm R}_{200}$. This box contains a sphere of radius $\rm R = 3.3R_{200}$, where $\rm R_{200}$ is physical radius within which density is 200 times the critical density of the Universe (McAlpine *et al.* 2016). According to Mamon *et al.* (2004) the first apocentre (backsplash) of galaxies in the Vigro cluster is at $1 < {\rm R_{vir}} < 2.5$. We define the infall radius for the same reason Oman and Hudson (2016) did: we want to avoid confusing galaxies that first enter the cluster and those which come back from the backsplash. Furthermore, using the definition of $\rm R_{vir}$ of Bryan and Norman (1998), being a radius of spherical volume in which the mean density is $\Delta_{\rm b}$ times the background density:

$$M_{\rm vir} = \frac{4}{3}\pi R_{\rm vir}^3 \Delta_b \rho_{\rm b} \tag{9}$$

with enclosed overdensity being $\rho_{\rm enc} = 360\rho_{\rm b}$. Viral radius, in terms of $\rm R_{200}$, can be expressed as $\rm 2.5R_{vir} \approx 3.3R_{200}$. We make this conversion since EAGLE provide tables for $\rm R_{200}$, $\rm R_{500}$ and $\rm R_{2500}$ and not for our definition of virial radius.

4071 satellite galaxies were found initially. We then collected merger trees of each satellite and filtered out those, which quenched before crossing $\rm 2.5R_{vir}$ (via "mass quenching" or internal quenching, or those quenched earlier in groups) and those which are not quenched at z = 0, resulting in 2347 galaxies. The final sample binned by $\rm t_{quench}$ and $\rm t_{infall}$, which are explained in the next section, are shown in Fig. 4.

We tried analysing RECALL0025N0752, which has 8× the resolution of REFL0100N1504 simulation. Due to small simulation box size, there were too few hosts that would satisfy our selection conditions. Ideally, we would investigate other high-resolution simulations, however there are no data available via the same interface, which would require substantial additional effort to begin analyzing. Time constrains of this project did not allow us to do so.

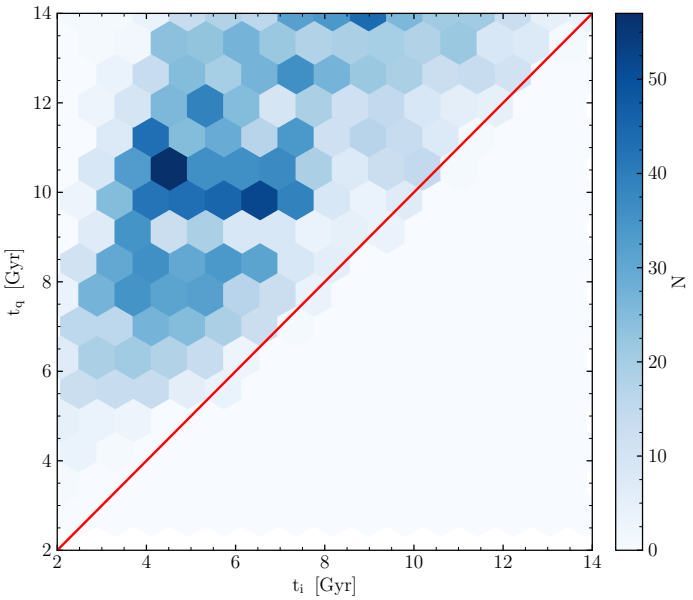

Figure 4: The final sample of satellite galaxies in RefL0100N1504 simulation, binned by their t_{quench} against t_{infall}. Vertical distance of a bin from the red line $t_{quench} = t_{infall}$, represents quenching timescale τ_q. Apparent clustering at $t_{quench} \approx 10$ Gyr is due to rather coarse time resolution of the simulation.

2.2 Quenching timescale

After a satellite has crossed $2.5R_{vir}$ (or $3.3R_{200}$) we consider it to be a part of the host subhalo and hence we record this time as t_{infall} for each satellite merger tree. We then follow its evolution and find the time when its SSFR crosses the SSFRcut threshold and label this t_{quench}. The difference between quenching time and the infall time is called "quenching timescale", $\tau_q = t_{quench} - t_{infall}$.

The definition for t_{quench} and t_{infall} are illustrated in Fig 5. Figures on the left show the radial separation history between the host and a satellite and R_{vir} of the host. R_{vir} grows as the host accretes mass over time. Figures on the right show the SSFR history and represent three general cases (top to bottom): (i) a satellite galaxy has SSFR $> 10^{-11}$ at z = 0 and hence is not considered to be quenched; (ii) a galaxy that has crossed the SSFRcut threshold at z = 0 and hence considered to be quenched and (iii) a galaxy in which SSFR dropped to 0 at $z \approx 0.5$; (iv) the SSFR drops below the SSFRcut threshold before the infall time, is not illustrated.

3 Results

In this section we will examine how the quenching timescale depends on infall time for different satellite mass ranges, then look at the dependence of the quenching timescale on properties of the satellite orbit and finally at how properties of the satellite itself affect its quenching timescale.

3.1 Infall time

We have computed τ_q and t_{infall} of each satellite and plotted them against each other to examine the general trends, which can be seen in Fig 6. Current time is at $t = 14$ Gyr and the Big Bang is at $t = 0$ Gyr. Each panel, except for top left, is split by stellar mass. Distributions in τ_q and t_{infall} are shown for each panel. It can be seen that there are considerably fewer galaxies

of higher stellar mass and their spread in τ_q is narrower, compared to the larger number of less massive satellites with wider spread in τ_q. More massive satellites also infall at later times, since they need more time to accrete that much mass.

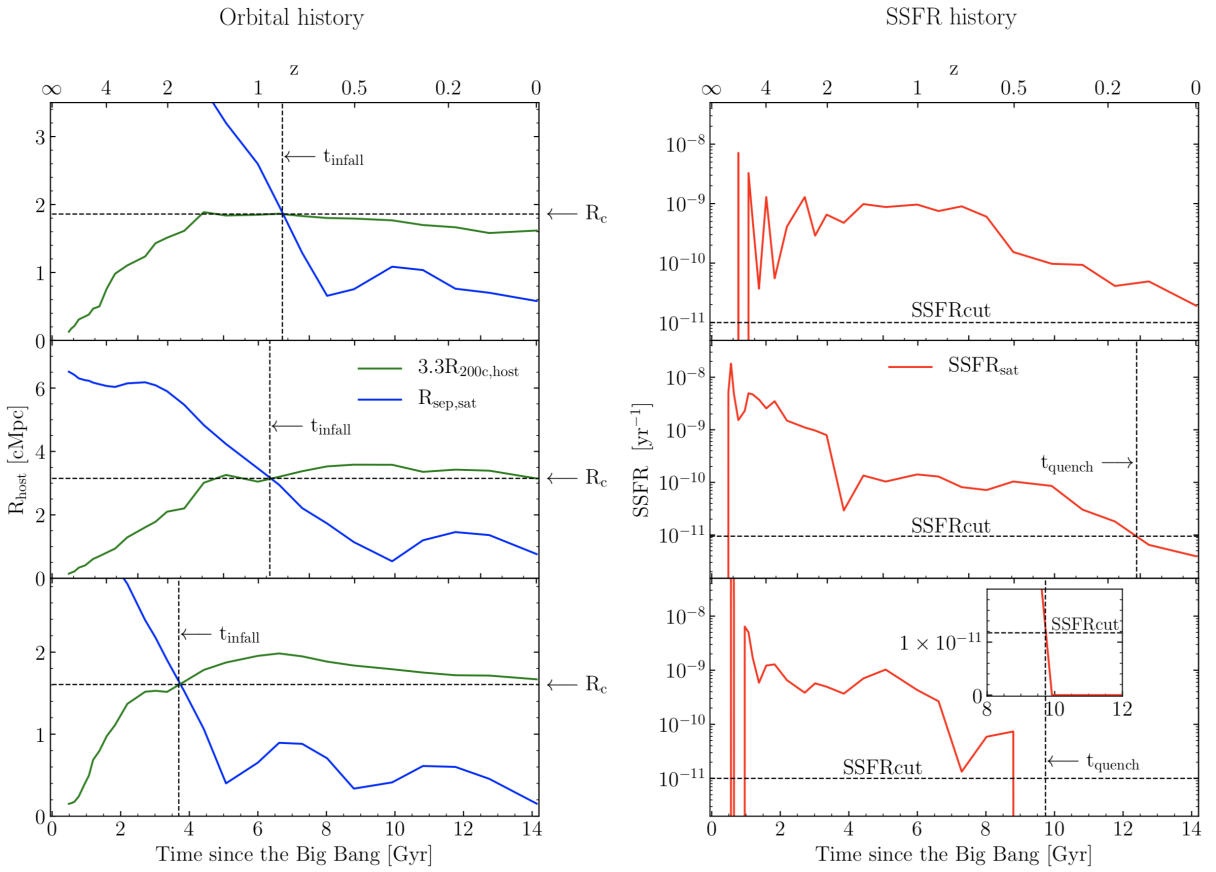

Figure 5: Orbital and SSFR history of three satellites. Panels on the left show radial separation between a host and its satellite. The infall time, t_{infall} is defined as time at which the satellite has crossed virial radius of the respective host at distance R_c. Panels on the right show the SSFR history of respective satellites. We define quenching time t_{quench} at a point when SSFR drops below 10^{-11} yr^{-1}. The top right panel shows a galaxy which has not quenched at z = 0 and hence was excluded from our final sample; middle panel shows SSFR of a galaxy that quenched after infall, but still has non-zero SSFR at z = 0; bottom panel shows a galaxy which has SSFR dropped to 0. A zoom-in shows a linear scale for SSFR, since 0 can not be represented on $\log_{10}$ scale.

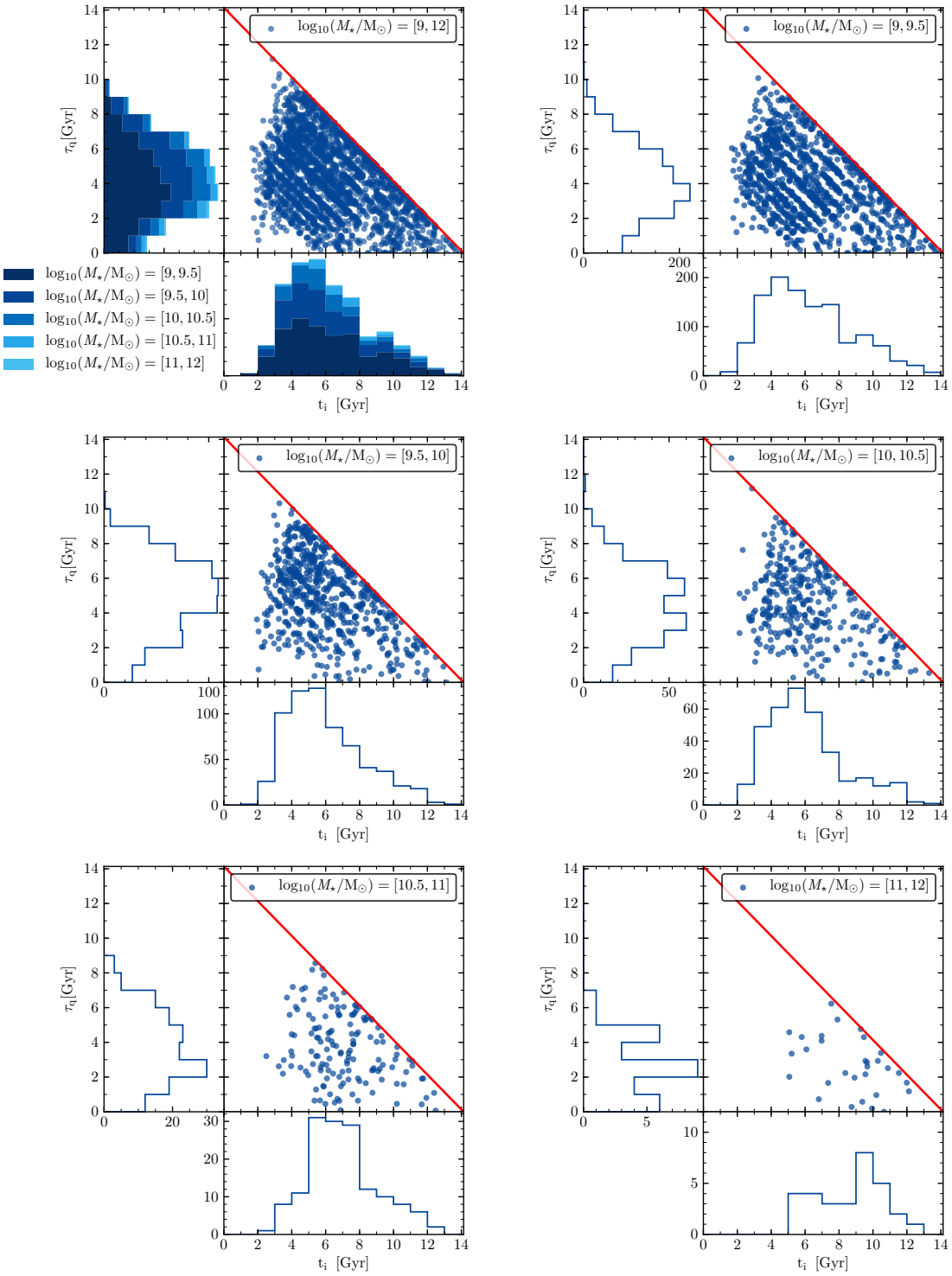

Figure 6: Quenching timescale as a function of infall time split by satellite stellar mass. Each plot is supported by τ_q and t_{infall} histograms. The Big Bang is at t = 0 Gyr and current time is at t = 14 Gyr. Top left panel shows the whole population, $\log_{10}(M_\star/M_\odot) = [9, 12]$. Colours in histograms represent satellites of different masses with dark blue indicating less massive satellites and light blue indicating more massive satellites. All other plots show τ_q–t_{infall} relation, split by stellar mass, which are indicated in the corresponding legends. The red line illustrates our selection criterion – satellites are only accepted if they quench after infall

3.2 τ_q peak

3.2.1 External/orbital properties

Now we will examine how orbital properties affect $\tau_{\rm q}$ at different satellite stellar masses. We compute $\tau_{\rm q}$ for each satellite galaxy and plot it against its mass. The median as a function of satellite stellar mass can be seen in Fig. 7. The sample is further separated by host mass in ranges $10^{13} < {\rm M_{host}/M_\odot} < 10^{14}$ and $10^{14} < {\rm M_{host}/M_\odot}$. Vertical bars show the interquartile range of $\tau_{\rm q}$, i.e. the spread of $\tau_{\rm q}$ in a given mass bin, and not an error or uncertainty. We observe a trend of satellites having shorter $\tau_{\rm q}$ when they orbit more massive hosts, compared to those which orbit lighter hosts. In both cases there is a peak in quenching timescale around satellites of mass ${\rm M_\star/M_\odot} \approx 10^{9.75} - 10^{10}$, compared to Fillingham *et al.* (2015), who found a peak at ${\rm M_\star/M_\odot} \approx 10^{9}$. Bottom panel illustrates stellar mass distribution of satellites. (The sample above ${\rm M_\star/M_\odot} > 10^{11}$ is strongly affected by shot noise due to low number counts.)

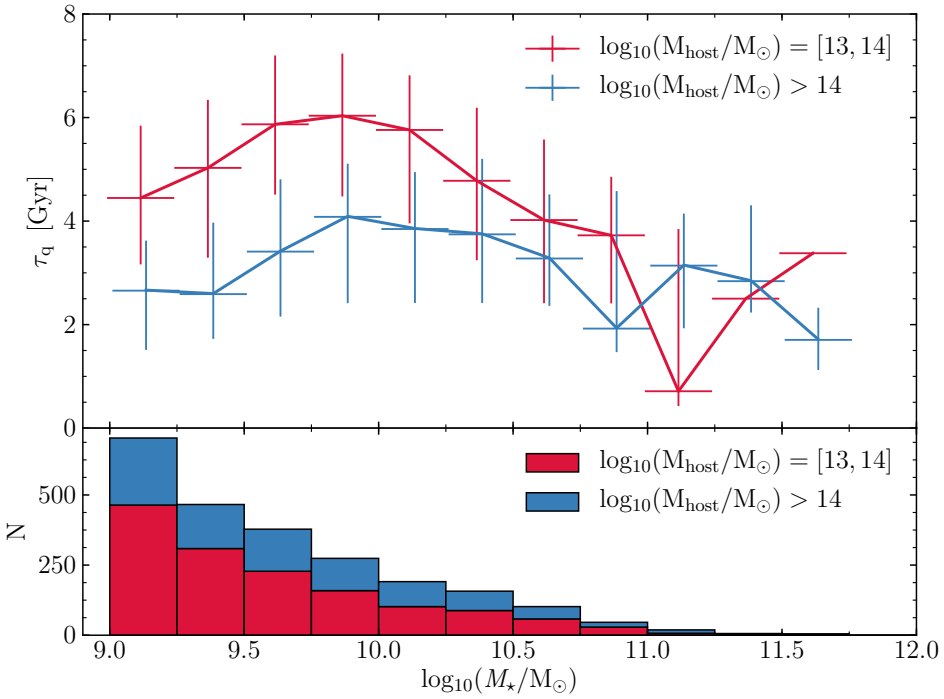

Figure 7: Quenching timescale distribution (QTD) of satellites split by host mass. Satellites that orbit more massive hosts consistently have shorter $\tau_{\rm q}$ compared to the ones that orbit lighter hosts. However, regardless of the mass of the host, a general trend can be observed: positive slope in $\tau_{\rm q}$ for satellites with low stellar mass; negative slope for satellites with high stellar mass; a peak at intermediate stellar masses. Bottom panel shows a stellar mass distribution of the satellties.

$\rm Q_1$, $\rm Q_2$, $\rm Q_3$ and $\rm Q_4$ mean first, second, third and forth quartiles of the population, respectively. Splitting the population by orbital speed at the pericentre, $\rm v_{peri}$ produces an intuitive result: satellites that have a higher $\rm v_{peri}$ ($\rm Q_3 + Q_4$) have shorter $\tau_{\rm q}$ and satellites with lower $\rm v_{peri}$ ($\rm Q_1 + Q_2$) have longer $\tau_{\rm q}$. This can likely be explained by RPS, which is dependant on $\rm v^2_{peri}$. The $\tau_{\rm q}$ – $M_\star$ relation is shown in Fig. 8 and the distribution of $\rm v_{peri}$, split by stellar mass, can be seen in Fig. 9. The distributions are similar across all stellar masses, which limits biases in the QTD.

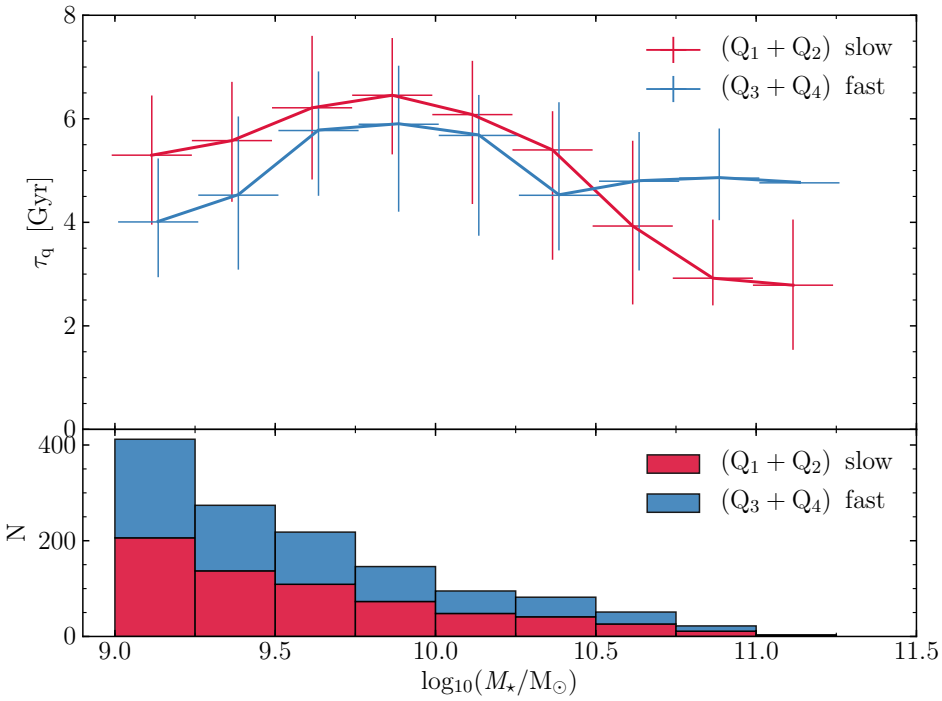

Figure 8: QTD, similar to Fig. 7, but split by the square of the speed at the first pericentre, v^2_{peri}, around hosts of mass range $\log_{10}(M_{host}/M_\odot) = [13, 14]$. $Q_1 + Q_2$ (Q for "quartile") are the "slower half" and $Q_3 + Q_4$ are the "faster half". Satellites that have higher orbital speeds consistently have shorter τ_q compared to slower satellites. The same overall trend is observed: intermediate mass satellites (both fast and slow) have longer τ_q, compared to lighter and heavier ones.

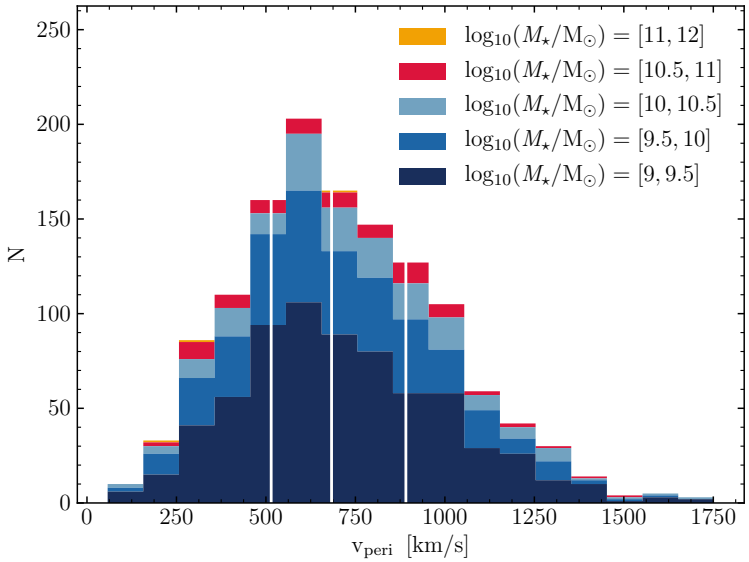

Figure 9: Distribution of v_{peri}, split by satellite stellar mass $M_\star$. The boundaries of the quartiles of the distribution are indicated by white stripes. The distribution is split up by stellar mass, as indicated in the legend.

Splitting the population by pericentric distance, r_{peri} can be seen in Fig. 10. The two populations lie close to each other, which does not summon any intuitive explanation. If the population with closer pericentric approach had a considerably lower τ_q we could have explained it with RPS, as it is dependant on ρ_{ICM}, which increases toward the host centre. However, it is not the case and currently we can not explain what is the main (if there is one) quenching mechanism, driving this small difference. The distribution of pericentric distances, split by stellar mass, is shown in Fig 11.

Due to the coarse time resolution of the simulation outputs, as can be seen in Fig. 5, r_{peri} is systematically overestimated. Pericentric approach that we read out will almost always be before or after the actual pericenter. This blurs the boundary between the upper and lower halves of the group (between lower two quartiles and upper two quartiles), but should preserve any overall trend. Same holds for maximum orbital speed, except it is systematically underestimated.

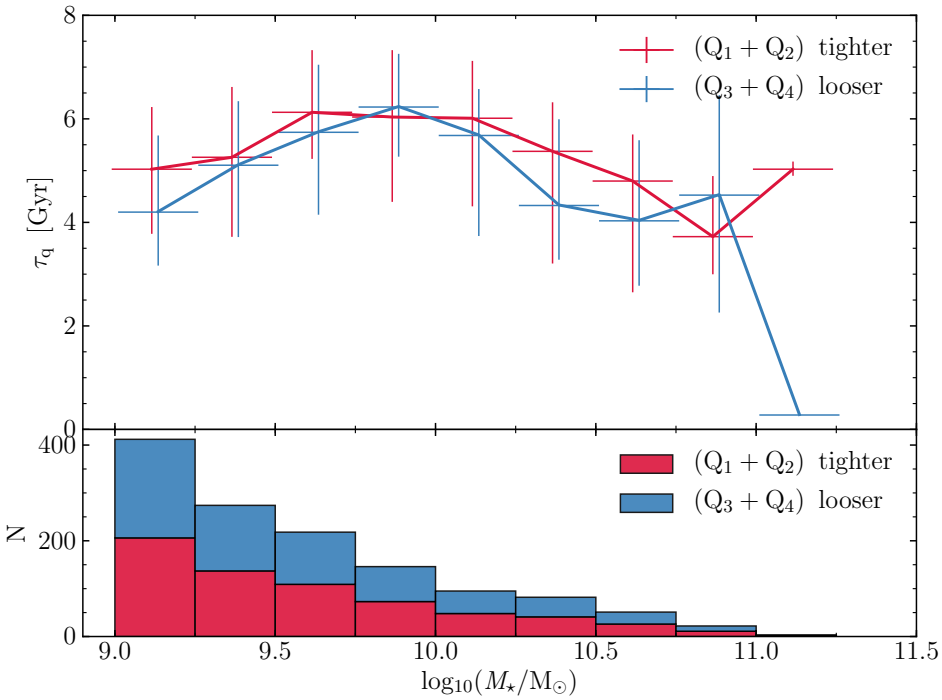

Figure 10: QTD, similar to Fig. 7, but split by the radial separation at first pericentric approach r_{peri} around hosts of mass range $\log_{10}(M_{host}/M_\odot) = [13, 14]$. $Q_1 + Q_2$ are the satellites with tighter orbits and $Q_3 + Q_4$ are the satellites with looser orbits. The split does not indicate a strong difference in the quenching times between the populations. The same overall trend holds: intermediate mass satellites have longer τ_q, compared to lighter and heavier ones.

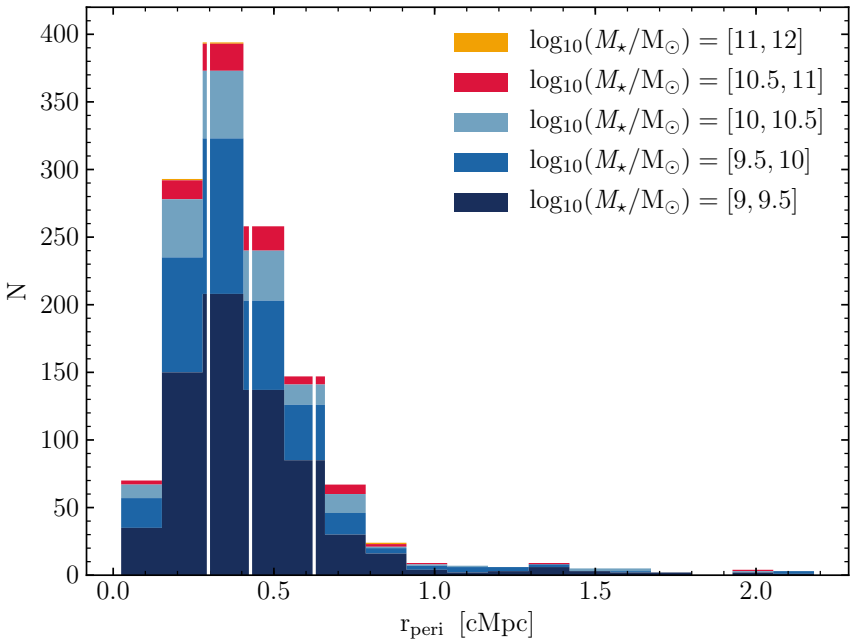

Figure 11: Distribution of r_{peri}, split by satellite stellar mass $M_\star$. The boundaries of the quartiles of the distribution are indicated by white stripes. The distribution is split up by stellar mass, as indicated in the legend.

3.2.2 Internal quenching

We also consider some internal properties. Comparing dense and diffuse satellites, as traced by projected physical radius enclosing half of the stellar mass, $R_{half,\star}$ (Fig. 12), we find that the split moved the peak by about -0.5 dex for the compact satellites. This suggests that it's important to consider how the properties of the satellite can change how it is affected by the host.

We also divide the sample according to the gas content at infall, $M_{gas}/M_\star$ at t_{infall} (top and bottom halves) demonstrates similar trend to the external influence: there is a peak in τ_q at intermediate masses, which can be seen in Fig. 13a. If we now consider top and bottom quarter, the peak disappears in galaxies with low $M_{gas}/M_\star$ ratio at infall (Fig. 13b) and is $\tau_q \approx 2$ Gyr for all the satellites. This is the lowest median for τ_q we have measured for any subsample.

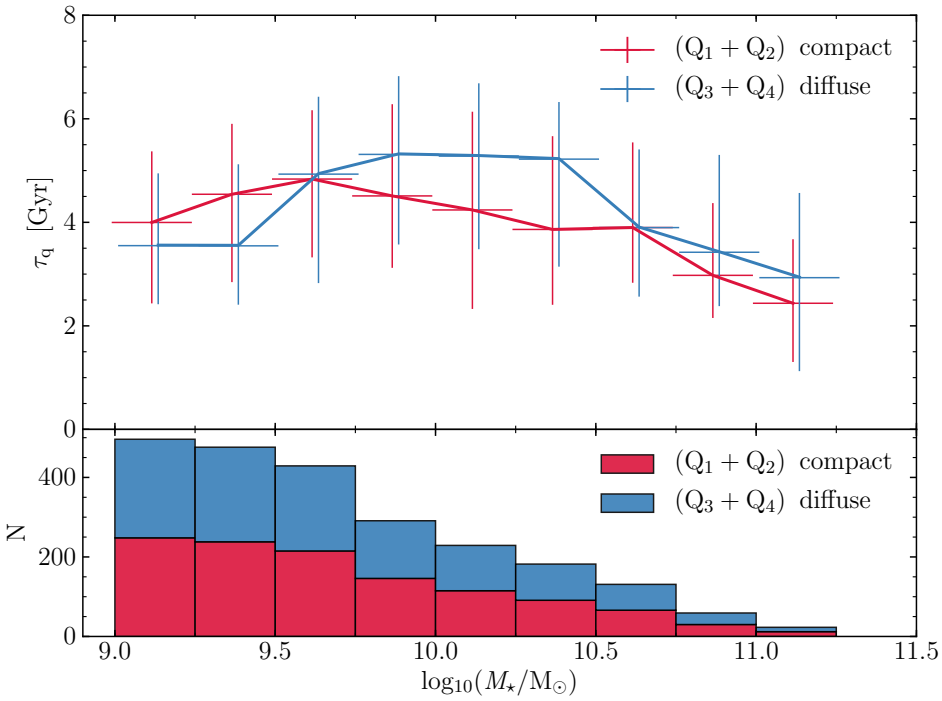

Figure 12: QTD split by $R_{half,\star}$. $Q_1 + Q_2$ are the compact satellites and $Q_3 + Q_4$ are the "diffuse" satellites. One can notice the peak moving to the left for the compact, which is suggests that density of a satellite somehow determines M_{crit}. Again, intermediate mass satellites have longer τ_q, compared to lighter and heavier ones.

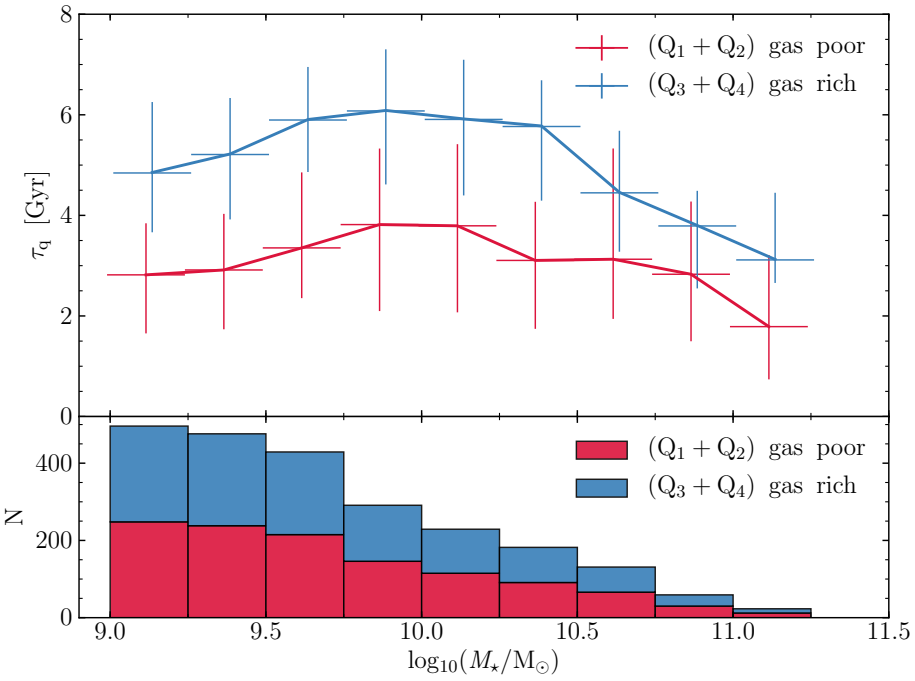

(a)

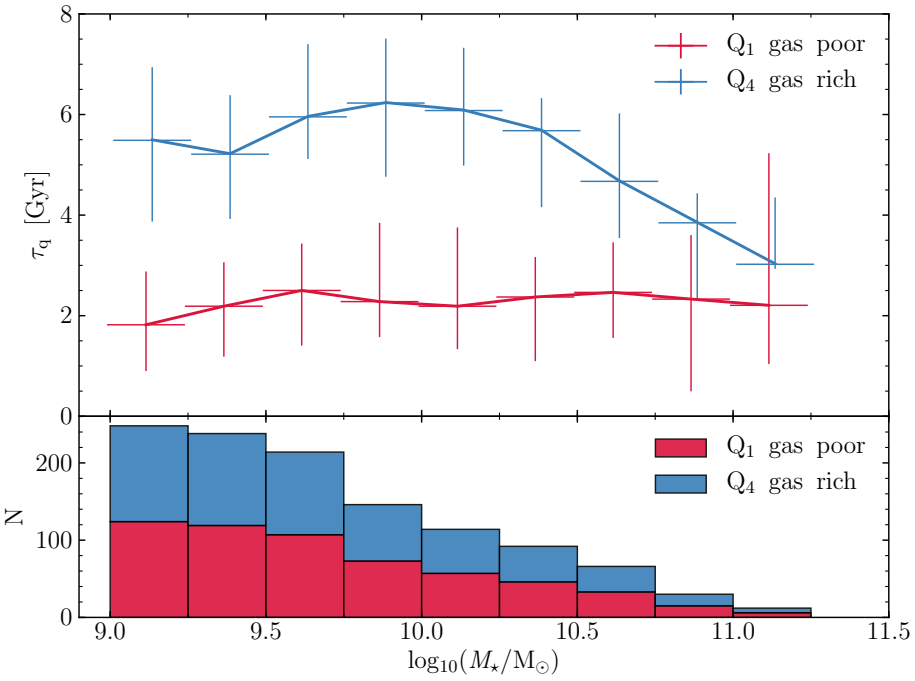

(b)

Figure 13: QTD, similar to Fig. 7, but split by $M_{gas}/M_\star$ at t_{infall}. (a): $Q_1 + Q_2$ are the gas poor satellites and $Q_3 + Q_4$ are the gas rich satellites. Intermediate mass satellites have longer τ_q, compared to lighter and heavier ones for both populations. (b): Q_1 are galaxies that almost depleted their reservoirs and Q_4 are gas rich satellites. The trend with intermediate mass satellites having longer τ_q holds for gas rich satellites. Gas poor satellites have more or less constant $\tau_q \approx 2$ Gyr across the whole range of stellar masses.

4 Discussion

4.1 The origin of the maximum in the quenching timescale at M_{crit}

Trends in τ_q–$M_\star$ relation are similar to the ones found by Fillingham *et al.* (2015). There is some intermediate stellar mass M_{crit} for which quenching seems least effective; there seems to be a mechanism that becomes more effective with *increasing* stellar mass of the satellite; there also seems to be a mechanism that becomes more effective with *decreasing* mass of satellites; where both slopes meet, the two mechanisms are less effective. The trend holds and quenching is more effective when satellites orbit more massive hosts, which is in line with an RPS-driven quenching scenario, since more massive hosts will have a denser ICM, which would make RPS more effective (eqn. 1). Similarly, the trend holds if the population in split by v_{peri}; satellites with higher v_{peri} will also be quenched more effectively due to RPS. We found a very weak trend for satellites with smaller r_{peri} to have longer quenching times.

Examining internal properties which then affect the interaction with the ICM shows some promising results. Firstly, splitting by $R_{half,\star}$ at $z = 0$ moved the peak towards lower masses by about 0.5 dex, which is the only property (which we tested) that displaced the peak, indicating that more compact satellites are affected differently to more diffuse satellites. Furthermore, the compact satellites have longer τ_q at lower stellar mass ranges; they have more dense discs which have stronger self-gravity (eqn. 2) and can more effectively resist RPS.

Splitting by $M_{gas}/M_\star$ also show intiutive results: galaxies with low amounts of gas quench faster, as they run out of fuel very quickly. The usual (for this thesis) trend holds for $(Q_1 + Q_2)/(Q_3 + Q_4)$ split. If we split the population by Q_1/Q_4, the gas poor satellites have their median in τ_q around 2 Gyr across all mass ranges. Interestingly, this is also the time it takes for a galaxy to reach pericenter from infall. This suggests that the pericentric approach is an important metric.

Medians of $M_{gas}/M_\star$ as a function of $M_\star$ at t_{infall} can be seen in Fig.14. Vertical lines are the first and third quartile of the distribution in each mass bin. Oort (1970) and Larson *et al.* (1980) argued that depletion time in spirals is much shorter than the Hubble time so there must be an influx of gas at least of that same rate as the gas is spent on producing stars. Examining $M_{gas}/M_\star$ as a function of stellar mass shows that there are low amounts of gas per unit solar mass in heavier satellites, so as they enter the ICM they get their gas depleted quickly, $\tau_q \approx 4$ Gyr (Fig. 13a), since it can not be replenished anymore. Lighter satellites, on the contrary, have large amount of gas, but also they have lower gravitational pull on it, hence they may lose it via RPS and/or feedback, with $\tau_q \approx 5$ Gyr. It appears that intermediate mass galaxies are in a regime where RPS and strangulation both become less effective: they can hold on to their gas/can shield from RPS and have enough gas to produce stars for the next ≈ 6 Gyr even while being strangled by the ICM.

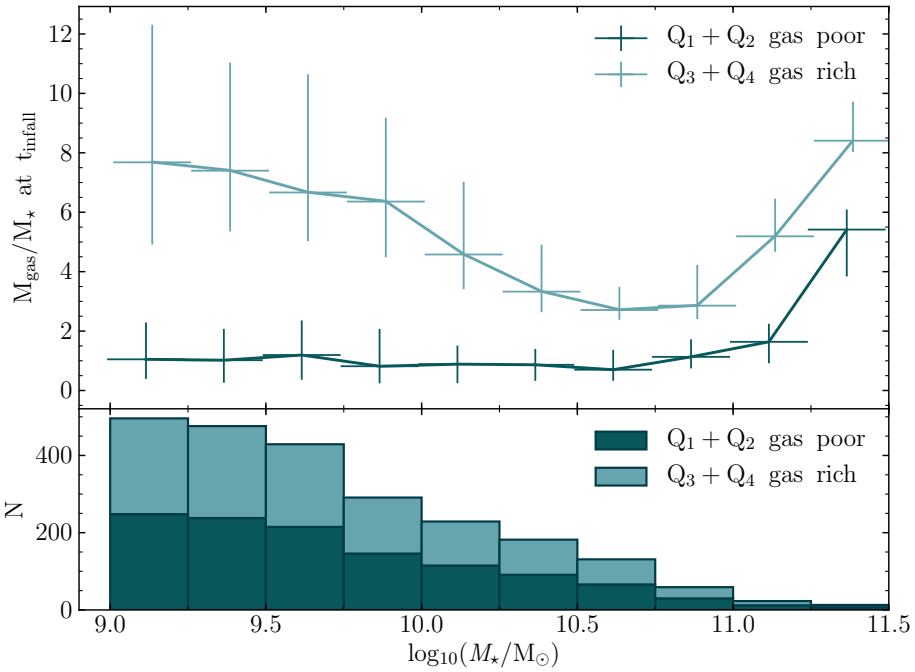

(a)

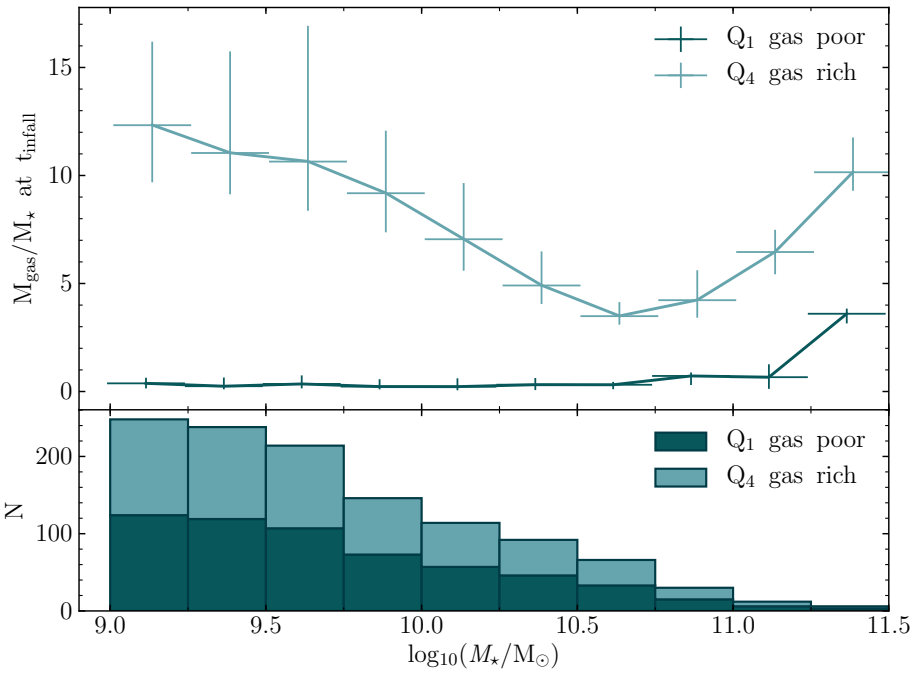

(b)

Figure 14: Medians of $M_{gas}/M_\star$ as a function of stellar mass in satellites. $(Q_1 + Q_2)/(Q_3 + Q_4)$ and Q_1/Q_4 splits are shown in figures (a) and (b) respectively. For gas rich satellites $(Q_3 + Q_4)$ in (a) and Q_4 in (b) fractional gas mass grows as the stellar mass decreases, starting form, $10^9 < M_\star/M_\odot \approx 10^{10.75}$. Satellites with masses $M_\star/M_\odot > 10^{11}$ are typically the central galaxies of infalling groups; their large gas fractions come from the intra-group medium, whose gas is assigned to these galaxies by the group finder.

4.2 Negative slope

Regardless of the quenching mechanism, part of the explanation for the negative slope in τ_q for the heavier galaxies is because these have a small spread in τ_q (bottom right panel in Fig. 6) , and the spread increases with decreasing satellite stellar mass (top right panel in Fig. 6). And it must be small because we chose galaxies that have quenched at $z = 0$ but most massive galaxies take longer to assemble in the first place so the heavy galaxies preferentially infall at later times (interquartile range is shown as super- and subscript) $t_{infall} = 9.3^{+0.8}_{-2.3}$ Gyr and so they must have (relatively) short quenching time $\tau_q = 2.6^{+1.4}_{-0.9}$ Gyr in order to be included in our sample. Less massive galaxies, on the other hand, do not need as much time to form and hence they can have a larger spread in $\tau_q = 3.9^{+1.5}_{-1.4}$ Gyr with $t_{infall} = 5.9^{+1.9}_{-1.6}$ Gyr in order to be included in our sample. Since we plot medians and their spread, intermediate galaxies will have higher values for their medians $t_{infall} = 5.7^{+1.5}_{-1.2}$ Gyr and $\tau_q = 4.3^{+1.7}_{-1.4}$ Gyr, which will decrease with growing mass, hence the negative slope. The red line demonstrated our selection criterion – only the satellites that quench after the infall are included in our sample.

High mass satellites are affected by a selection bias, but it does not explain our results. We selected the galaxies with a narrow infall time at $t_{infall} \approx 6$ Gyr and repeated the experiment. The τ_q–$M_\star$ relation still had the same shape with slightly steeper gradients (negative slope for high mass satellites and positive slope for low mass satellites).

4.3 Butcher-Oelmer effect

Butcher and Oemler (1984) have shown that compact cluster at $z > 0.1$ have a significant fraction of blue galaxies, with the fraction increasing with the redshift. We can give a weak explanation to the B-O effect in the context of our results. Medians and interquarlite range of infall times and quenching timescales of the whole population are $t_{infall} = 5.34^{+1.5}_{-1.2}$ Gyr and $\tau_q = 4.5^{+1.6}_{-1.4}$ Gyr respectively. Very roughly, the population will become more and more redder after $t \approx t_{infall} + \tau_q \approx 10$ Gyr ($z \approx 0.4$) and will be completely quenched by $t \approx 14$ Gyr. Hence the B-O effect can be a consequence of the evolutionary timescales of the galaxies. Our selection criterion excluded galaxies that quenched before the infall time and those which have not quenched at $z = 0$, which are needed for an actual analysis to quantify the fraction of blue galaxies as a function of redshift.

5 Conclusion

We have found a peak in τ_q–$M_\star$ relation, similar to Fillingham *et al.* (2015). Although it is hard to compare them directly, since the original work has satellites that orbit hosts of different masses, including some inaccessible in the simulations we have used due to their limited resolution. It seems consistent with a scenario where satellites of different masses are affected by different mechanisms: lighter ones are affected by RPS; heavier ones are affected by strangulation and intermediate ones can effectively shield themselves from RPS while having a considerable amount of spare gas to continue from stars for ≈ 6 Gyr, even while being strangled by the ICM.

Orbital properties influence the quenching timescale across all stellar masses. Splitting the population by v_{peri}, M_{host} and r_{peri} we find that the trend of intermediate mass satellites having longer quenching time, compared to lighter and heavier counterparts is independent of r_{peri}, while v_{peri} and M_{host} show to have a noticeable difference in quenching timescales.

Subdividing our sample by internal properties, $R_{half,\star}$ and $M_{gas}/M_\star$, show that they can affect how the satellite will interact with the cluster environment. Especially, low mass satellites split by $R_{half,\star}$: it seems that the more compact satellites are more resilient to RPS (if we assume that RPS is the main quenching mechanism for the lighter satellites). Splitting by $M_{gas}/M_\star$ shows that galaxies with low amounts of gas will quench in $\tau_q \approx 2$ Gyr (which is the time it takes for the satellite to fall to its pericenter from $2.5R_{vir,host}$), regardless of its stellar mass.

Further work could use simulations with higher mass resolution which would allow to probe hosts and satellites of much lower masses. Measurements of the depletion timescale $\tau_{depl} = M_{gas}/SFR$, similar to what Fillingham *et al.* (2015) did, can be examined to determine how effective strangulation is without any other quenching mechanisms. It would also be interesting to robustly quantify the fraction of blue galaxies as a function of redshift to test the B-O effect.

Acknowledgements

I thank my supervisor, Kyle Oman, for countless discussions, suggestions and explanations of the subject. I also thank my other supervisor, Marc Verheijen, for valuable feedback and recommendations for this thesis.

References

1. I. K. Baldry *et al.*, *MNRAS* **373**, 469–483 (2006).
2. W. A. Baum, *PASP* **71**, 106–117 (1959).
3. M. R. Blanton *et al.*, *ApJ* **594**, 186–207 (2003).
4. G. L. Bryan, M. L. Norman, *ApJ* **495**, 80–99 (1998).
5. H. Butcher, J. Oemler A., *ApJ* **285**, 426–438 (1984).
6. R. A. Crain *et al.*, *MNRAS* **450**, 1937–1961 (2015).
7. A. Dressler, *ApJ* **236**, 351–365 (1980).
8. S. P. Fillingham *et al.*, *MNRAS* **454**, 2039–2049 (2015).
9. F. Fraternali, J. J. Binney, *MNRAS* **386**, 935–944 (2008).
10. A. Ghosh *et al.*, presented at the American Astronomical Society Meeting Abstracts, vol. 51, p. 228.01.
11. J. E. Gunn, I. Gott J. Richard, *ApJ* **176**, 1 (1972).
12. R. B. Larson, B. M. Tinsley, C. N. Caldwell, *ApJ* **237**, 692–707 (1980).
13. G. A. Mamon, T. Sanchis, E. Salvador-Solé, J. M. Solanes, *A&A* **414**, 445–451 (2004).
14. S. McAlpine *et al.*, *AC* **15**, 72–89 (2016).
15. R. Morganti, *Frontiers in Astronomy and Space Sciences* **4**, 42 (2017).
16. K. A. Oman, MA thesis, University of Waterloo, 2013.
17. K. A. Oman, M. J. Hudson, *MNRAS* **463**, 3083–3095 (2016).
18. J. H. Oort, *A&A* **7**, 381 (1970).
19. Planck Collaboration *et al.*, *A&A* **571**, A1 (2014).
20. M. Postman, M. J. Geller, *ApJ* **281**, 95–99 (1984).
21. T. Quinn *et al.*, *Overview of FOF* (`https://faculty.washington.edu/trq/hpcc/tools/fof.html`).
22. J. Schaye *et al.*, *MNRAS* **446**, 521–554 (2015).
23. V. Springel, *MNRAS* **364**, 1105–1134 (2005).
24. The EAGLE team, *arXiv e-prints*, arXiv:1706.09899 (2017).
25. A. R. Wetzel, J. L. Tinker, C. Conroy, F. C. van den Bosch, *MNRAS* **432**, 336–358 (2013).